

Fully solvable finite simplex lattices with open boundaries in arbitrary dimensions

Ievgen I. Arkhipov^{1,*}, Adam Miranowicz^{2,3,4}, Franco Nori^{2,3,5}, Şahin K. Özdemir⁶, and Fabrizio Minganti^{7,8}¹Joint Laboratory of Optics of Palacký University and Institute of Physics of CAS, Faculty of Science, Palacký University, 17. listopadu 12, 771 46 Olomouc, Czech Republic²Theoretical Quantum Physics Laboratory, Cluster for Pioneering Research, RIKEN, Wakoshi, Saitama 351-0198, Japan³Quantum Information Physics Theory Research Team, Quantum Computing Center, RIKEN, Wakoshi, Saitama 351-0198, Japan⁴Institute of Spintronics and Quantum Information, Faculty of Physics, Adam Mickiewicz University, 61-614 Poznań, Poland⁵Physics Department, The University of Michigan, Ann Arbor, Michigan 48109-1040, USA⁶Department of Engineering Science and Mechanics, and Materials Research Institute (MRI), The Pennsylvania State University, University Park, Pennsylvania 16802, USA⁷Institute of Physics, Ecole Polytechnique Fédérale de Lausanne (EPFL), CH-1015 Lausanne, Switzerland⁸Center for Quantum Science and Engineering, Ecole Polytechnique Fédérale de Lausanne (EPFL), CH-1015 Lausanne, Switzerland

(Received 12 June 2023; revised 11 September 2023; accepted 22 September 2023; published 26 October 2023)

Finite simplex lattice models are used in different branches of science, e.g., in condensed-matter physics, when studying frustrated magnetic systems and non-Hermitian localization phenomena; or in chemistry, when describing experiments with mixtures. An n -simplex represents the simplest possible polytope in n dimensions, e.g., a line segment, a triangle, and a tetrahedron in one, two, and three dimensions, respectively. In this work, we show that various fully solvable, in general non-Hermitian, n -simplex lattice models with open boundaries can be constructed from the high-order field-moments space of quadratic bosonic systems. Namely, we demonstrate that such n -simplex lattices can be formed by a dimensional reduction of highly degenerate iterated polytope chains in ($k > n$)-dimensions, which naturally emerge in the field-moments space. Our findings indicate that the field-moments space of bosonic systems provides a versatile platform for simulating real-space n -simplex lattices exhibiting non-Hermitian phenomena, and it yields valuable insights into the structure of many-body systems exhibiting similar complexity. Among a variety of practical applications, these simplex structures can offer a physical setting for implementing the discrete fractional Fourier transform, an indispensable tool for both quantum and classical signal processing.

DOI: [10.1103/PhysRevResearch.5.043092](https://doi.org/10.1103/PhysRevResearch.5.043092)

I. INTRODUCTION

Simplex lattice models are used in various fields of science. In physics, they can describe antiferromagnetic Ising models [1–3] and non-Hermitian localization phenomena [4–7]; in chemistry, simplex lattices describe blending processes in multicomponent systems [8]; and in biology, they are used to model arrays of myosin filaments in higher vertebrate muscle packs [9]. A simplex is the simplest possible polytope in a given dimension, such as a line segment, triangle, and tetrahedron in one-dimensional (1D), 2D, and 3D spaces, respectively. Polytopes generalize polyhedra in arbitrary dimensions [10], and they have also been widely used in condensed-matter physics [11].

Finding the full and exact set of eigenvalues and eigenvectors of finite lattice models in any dimension is a difficult task. While there has been significant progress in finding exact

algebraic solutions for certain classes of periodic systems [12–16], as well as multidimensional Hermitian lattices [16], obtaining an analytical expression for the eigenspectrum of finite simplex nonperiodic (i.e., with open boundaries) systems remains challenging [17].

Finding new classes of solvable models is also important for benchmarking advanced numerical methods [18,19]. In addition to their mathematical value, the practical implementation of discovered exactly solvable lattice models in experiments holds significant importance, allowing us to gain valuable insights into the nature and behavior of seemingly complex physical systems.

Here we present an analytical solution for the eigenspectrum of finite n -simplex lattice models with open boundaries in *arbitrary* ($n \geq 1$) dimensions, which, most importantly, can naturally emerge in the field-moments (FMs) space of bosonic systems, and thus can be immediately simulated with state-of-the-art experimental setups. In this context, the term *open boundaries* implies the absence of periodic boundary conditions on such lattices.

At the heart of the proposed solution is the fact that these n -simplex lattices can be generated by a dimensional reduction of higher-dimensional iterated polytope chains (IPCs) into low-dimensional iterated simplex chains (ISCs), which are formed in the bosonic FMs space. This space folding can

*ievgen.arkhipov@upol.cz

be considered as a special projection of k -polytopes on an n -dimensional hypersurface, with a subsequent relabeling of the vertex and link weights of a formed lattice. The procedure thus echoes the cut-and-project method, used for obtaining quasicrystalline structures from higher-dimensional regular crystals [20–24], and it extends it to non-Hermitian systems. The exact eigenspectrum for the formed n -simplex lattices can then be readily attained by exploiting the tensor-product-states character of the eigenfunctions of IPCs.

The present study also generalizes the eigendecomposition of certain tridiagonal matrices [25,26], used to describe, e.g., angular momentum of quantum light and a number of various photonic non-Hermitian 1D simplex lattices [27,28]. The findings thus can pave the way for the study of nontrivial non-Hermitian effects in high-dimensional simplex structures.

Our results have potential applications in quantum simulations of non-Hermitian systems. The experimental observation of various many-body phenomena in engineered lattices remains challenging due to the difficulty in controlling all system parameters [29]. Our proposed method offers a promising solution to this problem, as it can be implemented using the FMs space of simple bosonic systems [30]. The FMs space serves as a universal tool, which can provide a broad variety of physical quantities not only in bosonic but also in fermionic systems, ranging from magnetoconductance of electrons to superconducting-normal phase boundaries [31–34]. That is, the studied n -simplex lattices, emerging in the FMs space of quadratic systems, can emulate certain lattice Hamiltonians, allowing for a much simpler, controllable, and scalable quantum simulation of high-dimensional lattices in the synthetic FMs space of few-boson systems [35–45]. The proposed procedure thus opens new avenues for the use of purely Hamiltonian quantum systems, such as linear optical quantum computers [46], for the simulation of nontrivial non-Hermitian phenomena [47].

Furthermore, as a technological application, we show that these simplex lattices, emerging in the FMs space, can also be exploited for implementing the discrete fractional Fourier transform (DFrFT). The DFrFT generalizes the ordinary discrete Fourier transform in a close analogy as the continuous fractional Fourier transform generalizes the continuous ordinary Fourier transform [48]. The DFrFT plays a central role in quantum and classical signal processing [49–51]. Namely, we demonstrate that these lattice structures can be mapped to the operator space of quantum angular momentum, which is used for implementation of DFrFT [49].

This paper is organized as follows. In Sec. II, we elaborate on the method for constructing the finite simplex lattices with a harmonic spectrum, which naturally appear in the FMs space of quadratic systems. Then, we describe in detail the geometry of these simplex structures, and we present an exact solution for their eigenspace. In Sec. III, we discuss the potential and significance of the revealed n -simplex lattices, highlighting their relevance in both theoretical and practical applications. Conclusions are drawn in Sec. IV.

II. THE METHOD

To explain the idea of the proposed method for constructing fully solvable harmonic finite simplex lattices, we first

consider the specific example of quadratic coupled bosonic modes, where the FMs space gives rise to the IPCs structure. That is, we first study the composition of the evolution matrices governing the dynamics of FMs of this quadratic Markovian system, and then we show that the m -series of evolution matrices, governing the i th-order FMs ($i = 1, \dots, m$), can be associated with the corresponding m -chain of high-dimensional polytopes, whose highly degenerate eigenspace is formed by tensor-product states. Following that, we briefly outline a dimensional reduction procedure of the highly degenerate space of the IPCs, leading to the formation of exactly solvable ISCs that can emulate real-space n -simplex lattices.

A. Evolution matrices governing high-order field-moments space

Let us consider a quadratic, in general non-Hermitian, N -mode system, whose Hamiltonian is

$$\hat{H} = \sum_{m,n} H_{mn} \hat{\Psi}_m^\dagger \hat{\Psi}_n \quad (1)$$

with $\hat{\Psi}_j$ the j th element of the Nambu vector,

$$\hat{\Psi} = [\hat{a}_1, \hat{a}_2, \dots, \hat{a}_N, \hat{a}_1^\dagger, \hat{a}_2^\dagger, \dots, \hat{a}_N^\dagger]^T, \quad (2)$$

where \hat{a}_k (\hat{a}_k^\dagger) is the annihilation (creation) operator of the mode k , obeying $[\hat{a}_k, \hat{a}_l^\dagger] = \delta_{kl}$ and $[\hat{a}_k, \hat{a}_l] = 0$. From the Heisenberg equations of motion, one can easily write down the equations for the dynamics of the first-order field moments $\langle \hat{\Psi} \rangle$ as

$$\frac{d}{dt} \langle \hat{\Psi} \rangle = M_1 \langle \hat{\Psi} \rangle, \quad (3)$$

where M_1 is the corresponding evolution matrix for the first-order FMs. Note that the same procedure can be straightforwardly extended to Hermitian operators as well as to, e.g., bosonic quadrature operators.

The analytical form of an evolution matrix governing the dynamics of any higher-order FMs can be obtained by exploiting properties of matrices formed by Kronecker sums [47]. Namely, any m th-order FM vector, constructed from the moments of the tensor products of the Nambu vector $\hat{\Psi}$, i.e., $\langle \bigotimes_1^m \hat{\Psi} \rangle$, is governed by the evolution matrix M_m , which is obtained from M_1 as follows:

$$\frac{d}{dt} \left\langle \bigotimes_1^m \hat{\Psi} \right\rangle = M_m \left\langle \bigotimes_1^m \hat{\Psi} \right\rangle \quad \text{with} \quad M_m = \bigoplus_1^m M_1, \quad (4)$$

where symbols \otimes and \oplus stand for the Kronecker tensor product and sum, respectively. For more details, see Appendix A and Ref. [52]. For simplicity, in Eq. (4) we ignore any possible presence of inhomogeneous parts stemming from quantum noise. Note that for odd-order non-Hermitian FMs, the inhomogeneous part is always absent for weakly coupled Markovian systems, while for even-order Hermitian FMs, the noise might enter the right-hand side of Eq. (4), though it does not affect the frequency spectrum of a system [53].

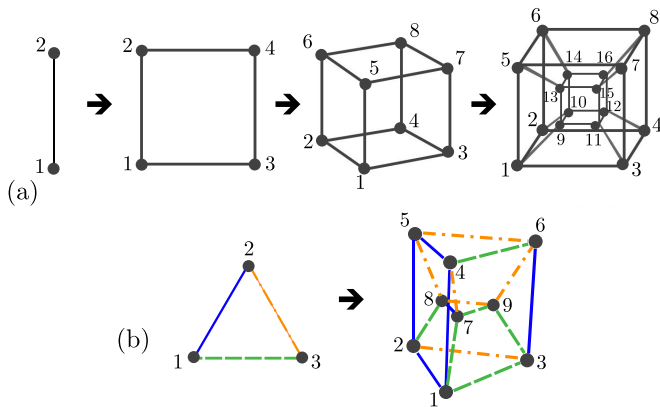


FIG. 1. Iterative polytope chains in the field-moments (FMs) space of bosonic (a) dimers and (b) trimers, formed by the Cartesian products of 1-polytope (a line) and 2-polytope (a triangle), respectively. (a) 1-polytope (a line) for the first-order FMs of the dimer; 2-polytope (a square) for its second-order FMs; 3-polytope (a cube) for its third-order FMs; and 4-polytope (a hypercube, shown via its 3D Schlegel diagram) for its fourth-order FMs. (b) 2-polytope (a triangle) for the first-order FMs of the trimer, and 4-polytope (a 4D duoprism, shown via its 3D Schlegel diagram) for its second-order FMs. Numbered vertices correspond to the elements of the FMs vector $\langle \otimes_1^k \hat{\Psi} \rangle$, with vertex potentials and the link weights corresponding to the diagonal and off-diagonal elements of the related evolution matrix M_k , respectively.

B. Iterated polytope chains in the field-moments space of bosonic systems

A chain of m evolution matrices $M_1 \rightarrow M_2 \rightarrow \dots \rightarrow M_m$, in Eq. (4), induces an IPC of m i_k -polytopes,

$$P_{i_1} \rightarrow P_{i_2} \rightarrow \dots \rightarrow P_{i_m}, \tag{5}$$

produced by iterated Cartesian powers of P_{i_1} ; namely,

$$P_{i_k} = (P_{i_1})^k,$$

where P_{i_1} is actually a simplex, i.e., the simplest polytope in a given dimension associated with the first-order FMs space.

The dimension of a polytope P_{i_k} is $k \times d$, where d is the dimension of the P_{i_1} polytope. The vertices of a polytope P_{i_k} are given by the elements of the FMs vector $\langle \otimes_1^k \hat{\Psi} \rangle$. The vertex potentials and link weights are determined by the diagonal and off-diagonal elements of the matrix M_k , respectively. Moreover, because the matrix M_k inherits the symmetry of M_1 , according to Eq. (4), the links in P_{i_k} preserve the symmetry of those in the polytope P_{i_1} . Note that, in general, the polytope links can be asymmetric, i.e., with two different weights in opposite directions, if the FMs evolution matrices are non-symmetric.

For instance, in the case of a symmetric bosonic dimer, an evolution matrix M_1 can be associated with a 1D polytope P_1 , i.e., a line, formed by two vertices and one edge [see Fig. 1(a)]. A 2-polytope P_2 , corresponding to M_2 , then represents a square. As a result, one obtains an m -hypercube, describing the m th-order FMs space, whose associated matrix is M_m [see Fig. 1(a)]. Figure 1(b) illustrates the first two polytopes corresponding to the first- and second-order FMs of a symmetric three-mode system.

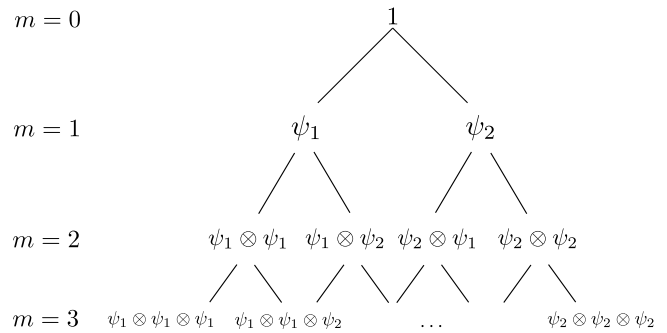


FIG. 2. Tensor-products tree of the eigenvectors of the evolution matrices M_m (with $m = 0, 1, 2, 3$) for a quadratic dimer, according to Eq. (6). The index $m = 0$ corresponds to the identity element. This tree is a solution for the iterative polytope chains in Fig. 1(a).

C. Tensor product eigenspace for iterated polytope chains

Here we discuss the eigenspace of the evolution matrices M_m associated with IPCs. Equation (4) implies that one can determine a complete eigendecomposition of the matrix M_m , governing m th-order FMs, knowing the eigenvalues and eigenvectors of the matrix M_1 , and, therefore, the eigenspace of the corresponding i_m -polytope (see Fig. 2 and Appendix A for details). Namely, the eigenvectors of the matrix M_m are found via all $(2N)^m$ combinations of the tensor products of the eigenvectors $\psi_j^{(1)}$, $j = 1, \dots, 2N$ of the matrix M_1 , together with the harmonic eigenvalues

$$\psi_{i_1, i_2, \dots, i_m}^{(m)} = \psi_{i_1}^{(1)} \otimes \dots \otimes \psi_{i_m}^{(1)}, \quad \lambda_{i_1, i_2, \dots, i_m}^{(m)} = \sum_{k=1}^m \lambda_{i_k}^{(1)}, \tag{6}$$

where each index $i_k = 1, \dots, 2N$ for each $k = 1, \dots, m$, and $\lambda_{i_k}^{(1)}$ are the eigenvalues of the matrix M_1 (see Appendix A).

The expression in Eq. (6) implies that the FMs space, associated with IPCs, can exhibit a large extra algebraic (diabolic) degeneracy, which is rapidly increasing with the FMs order. In all subsequent discussions, unless stated otherwise, we will call algebraic degeneracy the extra degeneracy linked with the construction of the IPCs. We will not refer to the other types of algebraic degeneracies, including those that are intrinsically associated with the spectrum of the generating matrix M_1 . The algebraic degeneracy stems from the fact that the different combinations of the eigenvalues λ_{i_k} may result in the same sum in Eq. (6), but may correspond to different eigenvectors. One can then straightforwardly calculate the algebraic degeneracy D for a given eigenvalue $\lambda_{i_1, i_2, \dots, i_m}^{(m)}$, as

$$D(\lambda_{i_1, i_2, \dots, i_m}^{(m)}) = \frac{m!}{n_{i_1}! n_{i_2}! \dots n_{i_m}!}, \tag{7}$$

where n_{i_k} denotes the number of times the index i_k appears in Eq. (6).

Noticeably, this diabolic degeneracy, originating in the IPCs eigenspace, can lead to a nontrivial interplay between diabolic points and exceptional points [54], provided that an evolution matrix M_1 possesses the latter. This can result in the formation of hybrid diabolically degenerate exceptional points (see Appendix C for details and also Ref. [53]). And while it may be challenging to directly access and utilize the properties of such hybrid degeneracies in the FMs space,

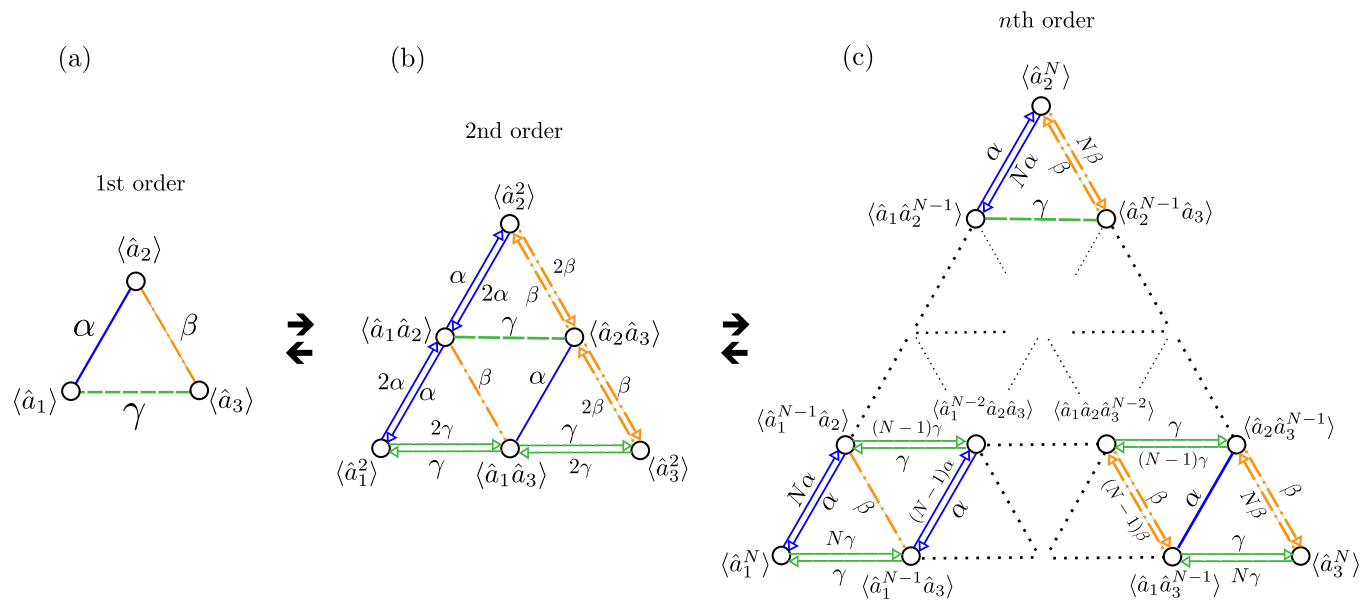


FIG. 3. Formation of iterative simplex chains (ISCs) by folding iterative polytope chains in the FMs space of bosonic three-mode systems. (a) A 2-simplex, i.e., a triangle, formed in the first-order FMs, which coincides with the P_1 polytope. The links, denoted by α , β , γ of different colors, correspond to the coupling strengths between the three FMs, according to Eq. (10). (b) ISC in the second-order FMs space. By folding the corresponding symmetric 4-polytope in Fig. 1(b), one arrives at an asymmetric triangular 2-simplex consisting of six vertices, according to Eq. (8). (c) ISC in the N th-order FMs space. The ISCs thus form a finite triangular non-Hermitian lattice with $(N+1)(N+2)/2$ vertices in the high-order FMs space. Formally, the presented 2-simplex chain can be considered in a reversed order, that is, a lattice in panel (c) can be reduced into a lattice in panel (a), which highlights the simple origin of the seemingly complex lattice in (c). Note that such formed asymmetric simplex lattices in the FMS of quadratic bosonic systems can be additionally symmetrized (see Appendix E for details).

they can be engineered and probed with relative ease in the spectrum of real-space systems exhibiting unique dynamical features [55].

D. Dimensional reduction of iterated polytope chains to iterated simplex chains, and the formation of finite simplex lattices

As mentioned above, the extra algebraic degenerate space in IPCs stems from the tensor-product-states nature of the FM vectors $(\otimes_1^m \hat{\Psi})$. Indeed, in a simple case of a linear dimer consisting of interacting fields, described by \hat{a}_1 and \hat{a}_2 , the system dynamics for the FMs $\langle \hat{a}_1 \hat{a}_2 \rangle$ and $\langle \hat{a}_2 \hat{a}_1 \rangle$ is the same, though both of these moments appear in the FMs vector $(\otimes^2 \hat{\Psi})$ by construction. However, one can effectively eliminate this redundant degeneracy by reducing $[(2N)^m \times (2N)^m]$ -dimensional evolution matrices M_m , describing k_m -polytopes, to low-dimensional effective matrices M_m^{eff} of the size

$$S_m(2N) = \frac{(2N+m-1)!}{m!(2N-1)!} < (2N)^m. \quad (8)$$

The expression for S_m is the standard formula for *combinations with repetition*, which leaves only nonequivalent FMs in the description of the FMs time evolution.

The projection of the matrix M_m onto M_m^{eff} can be generally represented as

$$M_m^{\text{eff}} = TL^\dagger M_m RT^{-1}, \quad (9)$$

where L and R are $(2N)^m \times S_m(2N)$ rectangular matrices comprised by the left and right eigenvectors of the matrix M_m , respectively. They project the matrix M_m onto its low

S_m -dimensional nondegenerate eigenspace, and where T is an $S_m \times S_m$ similarity transformation, e.g., a rotation, which allows us to write M_m^{eff} in an arbitrary basis (see Appendix B for more details). Since the eigenspace of the matrix M_m can be readily calculated in Eq. (6), one then immediately obtains the eigenspace of the reduced matrix M_m^{eff} .

Interestingly, the series of effective evolution matrices

$$M_1^{\text{eff}} \rightarrow M_2^{\text{eff}} \rightarrow \dots \rightarrow M_m^{\text{eff}}$$

can now be associated with an ISC, in analogy with Eq. (5). In other words, the dimensional reduction of evolution matrices $M \rightarrow M_{\text{eff}}$ is accompanied by the space reduction of the corresponding IPC into ISC. Moreover, such ISCs are defined in the same dimensional space as the simplex (polytope) P_1 .

Recall that for the first-order FMs, the polytope P_1 is actually a simplex. For instance, for a dimer, whose 1-simplex P_1 is a 1D line segment [see Fig. 1(a)], its ISC defines a line consisting of $[S_m(2) = m+1]$ vertices in the reduced m th-order FMs space. Accordingly, for a trimer, with P_1 being a triangle, i.e., a 2-simplex [Fig. 1(b)], the ISC defines a triangular chain on a 2D plane (see Fig. 3). Similarly, the high-order FMs space of an n -mode system can be represented by $(n-1)$ -simplex chains.

This space reduction of IPCs into ISCs can formally be considered as a projection of k_m -polytopes onto an $(n-1)$ -dimensional hypersurface which is formed by n points corresponding to the m th order of n fields, i.e., $\langle \hat{a}_1^m \rangle, \langle \hat{a}_2^m \rangle, \dots, \langle \hat{a}_n^m \rangle$. After such a projection, a k_m -polytope is folded into an $(n-1)$ -simplex lattice with $S_m(n)$ vertices. The vertex and link weights of the formed simplex lattice are then assigned by the corresponding effective matrix M_m^{eff} . For

instance, for a dimer, the 1D-hypersurface (a line) is the main diagonal of the $(k_m = m)$ -hypercube formed by two “vertices” $\langle \hat{a}_1^m \rangle$ and $\langle \hat{a}_2^m \rangle$. As such, 2^m vertices of an m -cube are projected to $S_m(2) = (m + 1)$ vertices lying on the main diagonal with the vertex and link weights described by the effective matrix M_m^{eff} .

Importantly, the reduction of IPCs into ISCs results in the formation of finite n -simplex lattices, which do *not* possess translational symmetry, regardless of whether the underlying and generating matrix M_1 is symmetric or not (see also Sec. II E). This also implies that these constructed simplex structures can only describe *finite* lattices with *open* boundaries, because no periodic conditions can be imposed. The latter restriction evidently stems from the requirement that these lattices have a harmonic spectrum.

The finite lattices, emerging in the FMs space of quadratic bosonic systems, can additionally emulate various real-space and other synthetic lattice models described by (non-)Hermitian Hamiltonians, whose matrix representation is equivalent to some M_m^{eff} . *This means that a high-order FMs space of bosonic systems can be used to find exact solutions of various finite (non-)Hermitian lattice models in arbitrary dimensions.* In other words, if the geometry of an arbitrary Hamiltonian, which can be expressed via an n -simplex lattice (in a real or synthetic space), can be identified with that of the constructed simplex structures studied here (see Sec. II E and Appendix D for typical examples), one can then readily obtain its exact eigenspectrum. This observation constitutes one of the main results of our work. Note, however, that the state spaces and the physical meaning of the state vectors can substantially differ depending on the representation of the emulated Hamiltonian. In Sec. III, we additionally discuss the practical relevance and other potential physical scenarios, where these n -simplex lattices can occur and be effectively utilized.

E. Example: Exactly solvable finite triangular non-Hermitian lattices with open boundaries

To elaborate more on the above-described procedure of obtaining finite simplex lattices with open boundaries in the FMs space, as an example, let us consider a linear three-mode system. Assume that its first-order FMs vector $\langle \hat{\Phi} \rangle$, $\hat{\Phi} = [\hat{a}_1, \hat{a}_2, \hat{a}_3]^T$, is governed by the following symmetric evolution matrix [see also Fig. 3(a)]:

$$M_1 = \begin{pmatrix} 0 & \alpha & \gamma \\ \alpha & 0 & \beta \\ \gamma & \beta & 0 \end{pmatrix}. \quad (10)$$

The diagonal elements of M_1 can in general be complex-valued. The evolution matrix M_N , governing the dynamics of the N th-order FMs vector $\langle \otimes_1^N \hat{\Phi} \rangle$, is then obtained from M_1 according to Eq. (4). The M_N describes a highly degenerate $2N$ -polytope [the case for $N = 1, 2$ is shown in Fig. 1(b)]. This redundant degeneracy can be eliminated via the map $M_N \rightarrow M_N^{\text{eff}}$, which geometrically corresponds to the reduction of a symmetric $2N$ -polytope, with 3^N vertices, to a 2D ISC forming a finite non-Hermitian triangular lattice with

$$S_N(3) = (N + 1)(N + 2)/2$$

vertices (see Fig. 3). The non-Hermitian nature of such a formed lattice is highlighted by the arising asymmetry in vertex bonds which become direction-dependent.

One can see in Fig. 3 that by iteratively increasing the FMs order, the corresponding ISC are iteratively augmented by 2-simplexes (i.e., triangles), generating thus a triangular lattice. This emerging triangular lattice can mimic a real-space bosonic non-Hermitian Hamiltonian $M_N^{\text{eff}} \rightarrow H_{\text{eff}}^N$ written in a mode representation. We give an explicit expression for this Hamiltonian in Appendix D. Importantly, this triangular lattice model in Fig. 3(c) is exactly solvable, since the eigenspace of the matrix M_N^{eff} is readily obtained from M_N in Eq. (6) by applying the described projection.

Similarly, as was mentioned earlier, an m -dimensional hypercube, related to the m th-order FMs of a dimer, can be reduced to a 1D non-Hermitian chain [depicted as one of the external boundaries of the triangular lattice in Fig. 3(c)] which is described by a tridiagonal Sylvester matrix M_k^{eff} [28]. Moreover, for a four-mode system one attains a tetrahedral-octahedral honeycomb lattice (see Appendix D). It is straightforward to extend this procedure to arbitrary n -mode systems, whose FMs space can be described by the corresponding $(n - 1)$ -simplex lattices with open boundaries.

Note that one can try to symmetrize a non-Hermitian matrix M_m^{eff} by choosing an appropriate basis if any. For example, for a 2-simplex lattice, shown in Fig. 3, one can find such a basis where the corresponding reduced matrix M_m^{eff} becomes symmetric (see also Appendix E for details).

This analysis can also be straightforwardly extended to any kind of a (non-) Hermitian matrix, which defines the evolution of the first-order field moments (away from exceptional points [56]). As the simplex lattices are characterized by bidirectional couplings, the asymmetry in M_1 is simply reflected in the modification of the corresponding link weights. For instance, by modifying the single element $M_1(1, 2) = \eta$ in Eq. (10) (i.e., changing only the tunneling amplitude from the mode \hat{a}_1 to the mode \hat{a}_2), the weights of links, denoted by the blue-colored vectors at 45° in panels (b) and (c) of Fig. 3, become factorized by the new parameter η . The remaining link weights remain unchanged. The symmetry of the underlying matrix M_1 , which is explicitly reflected in its spectrum, then persists in any subsequent matrix M_m^{eff} , and, therefore, in the associated n -simplex structures. The latter property follows from the harmonic character of the spectrum of M_m^{eff} , constructed by the eigenvalues of M_1 . For instance, if the matrix M_1 possesses the chiral or parity-time (PT) symmetry, that symmetry is also present in the formed n -simplex lattices.

III. APPLICATIONS

A. Discrete fractional Fourier transform

Here we show that 1D simplexes provide a physical setting for the computation of the DFrFT in the FMs space of a photonic symmetric dimer. As was already demonstrated in Ref. [49], by mapping the matrix of the angular momentum operator J_x onto a real-space Hamiltonian, describing the 1D array of coupled waveguides, one can effectively implement the DFrFT of any input signal. Our goal here is to show that the effective matrix M_N^{eff} , which determines the evolution

of the N th-order FMs space of the symmetric dimer and is associated with a synthetic finite 1-simplex array, can be cast onto the J_x matrix.

Geometrically, this 1-simplex array can be represented as one of the three main outer sides of the 2D simplex in Fig. 3(c), e.g., by the outer left-hand side of the lattice, where the link weights factored by the parameter α . This 1D-chain of the 2D simplex describes the FMs interaction between the modes \hat{a}_1 and \hat{a}_2 , while eliminating the presence of the mode \hat{a}_3 [see Fig. 3(c)]. The elements of the $(N+1) \times (N+1)$ FMs evolution matrix M_N^{eff} then has the following Sylvester tridiagonal form [26,47] (see also Appendix C):

$$M_N^{\text{eff}}(j, k) = (N-j)\alpha\delta_{j,k-1} + j\alpha\delta_{j,k+1}, \quad (11)$$

with indices $j, k = 0, \dots, N$. The matrix M_N^{eff} can be transformed into the operator of the quantum angular momentum (up to a scaling factor 2α) via a similarity transformation:

$$J_x = S^{-1}M_N^{\text{eff}}S, \quad (12)$$

where the diagonal matrix S reads (see Appendix E)

$$S(j, j) = \prod_{k=1}^j \sqrt{\frac{M_N^{\text{eff}}(k, k-1)}{M_N^{\text{eff}}(k-1, k)}}, \quad (13)$$

with $S(0, 0) = 1$. The matrix J_x has the form

$$J_x(m, n) = \alpha[\sqrt{(j-m)(j+m+1)}\delta_{m+1,n} + \sqrt{(j+m)(j-m+1)}\delta_{m-1,n}]. \quad (14)$$

For simplicity, we keep the $(N+1) \times (N+1)$ matrix J_x in the standard form, where the indices m and n range from $-j$ to j in unit steps, and $N = 2j$. The parameter j is a positive integer or half-integer. Thus, the 1D simplex lattice, arising in the FMs space of a symmetric dimer, becomes *similar* to the operator space of the quantum angular momentum.

One of the outcomes, stemming from the above correspondence, is the ability to compute the DFrFT of real-space 1D signals in the *synthetic* FMs space of the dimer. This can be achieved, for instance, by appropriately preparing the initial quantum state of a dimer, whose input vector of the field moments can then emulate a given 1D real-space signal. Such a task can be achieved in quantum hardware through quantum optimal control algorithms, such as, e.g., the GRAPE [57] or CRAB [58] algorithms. Most importantly, since the FMs space is robust against any perturbations by construction, it makes the computation of DFrFT resilient to additional noise, which inevitably arises due to experimental imperfections when engineering 1D arrays in real space [49]. As an additional step in our study, it would be interesting to examine the potential of the revealed harmonic n -simplex lattices to serve as a general framework for implementing the DFrFT in arbitrary dimensions for any $n > 1$.

We note that the isomorphism between the angular momentum operators and bosonic creation and annihilation operators of two-mode systems is known in the literature by exploiting the Jordan-Schwinger transformations from which one can recover the same operator Lie algebra [59]. Here, however, and quite remarkably, we have unveiled the same angular-momentum–bosonic dimer correspondence without any references to the system operators defined on the Fock

Hilbert space, dealing *exclusively* with the geometry of c -number-valued FMs. Moreover, we extend this correspondence to arbitrary m -mode quadratic systems (see Appendix E for details). This also means that experimental simulations of angular momenta can also be directly implemented in the FMs space of a dimer without relying, e.g., on postselection procedures, which directly exploit the Jordan-Schwinger transformations in the photon-number space of the system operators [60], and which, therefore, are hard to realize in practice for many-photon systems.

B. Other applications

The possibility to engineer chiral and \mathcal{PT} -symmetric n -simplex structures also enables us to study various topological, localization, and order-disorder transition phenomena in high dimensions. Thanks to their harmonic spectrum, one can easily engineer high-dimensional simplex lattices with, e.g., exceptional points or even hybrid diabolically degenerate exceptional points [55] of an arbitrary degeneracy. It is well known that the presence of highly degenerate exceptional points may induce various non-Hermitian phase transitions [6,61]. In particular, in Ref. [28] we have already unveiled the emergence of the non-Hermitian skin effect in the synthetic space of a \mathcal{PT} -symmetric dimer, whose FMs space corresponds to the 1-simplex array. The latter observation thus necessitates a further study of the associated non-Hermitian phenomena that can occur in high-dimensional n -simplex lattices for arbitrarily large $n > 1$.

We note that compared to Ref. [28], here we explicitly give the recipe for the construction of arbitrary dimensional n -simplex lattices in the FMs space, and, moreover, we found a general solution for their eigendecomposition. In particular, we present an alternative spectral solution for tridiagonal Sylvester matrices, whose exact eigenspectrum has been obtained only recently [26]. Therefore, we believe that our findings could also motivate and be of interest for future research in related mathematical and theoretical fields.

In addition to the above-described possible theoretical and experimental applications of the given n -simplex lattices, they offer primarily a simple visual representation and give valuable insights into the structure of the FMs space of bosonic quadratic systems. This result, to the best of our knowledge, was not previously known. Additionally, the exact eigendecomposition of these simplex structures provides an alternative solution for the high-order FMs of quadratic systems, thus bypassing the need to invoke the Wick theorem [62].

IV. CONCLUSIONS

We have revealed the formation of nontrivial exactly solvable non-Hermitian harmonic finite lattice models with open boundaries in the FMs space of arbitrary quadratic bosonic n -mode systems. The spectrum of such lattices, represented by ISCs, can be readily obtained by knowing the spectrum of higher-dimensional matrices describing IPCs, which are much easier to compute by exploiting the simple eigenspace structure of the latter.

Our results extend and generalize the previous works in Refs. [25,26,28], and provide valuable insights into the underlying structure of many-body lattice systems exhibiting similar complexity. These findings can prompt further studies on the simulation of various *high-dimensional* lattice topological and localization phenomena in the FMs of multimode bosonic systems. The results can also be directly utilized for finding high-order FMs of quadratic systems even without invoking the Wick theorem.

One of our main observations in this study is that some lattice structures, which look complex at first glance, can originate from simple low-dimensional arrangements. This insight, thus, resonates with the concept of quasicrystalline structures, which can be obtained through the projection of high-dimensional regular crystals onto certain hyperplanes [63], or it can even draw parallels with fractal-like formations, where complex geometric patterns arise from much simpler geometric objects via iterative transformations [64].

These findings also enable a potential application of n -simplex lattices to provide a physical setting for realizing an arbitrary dimensional DFrFT either directly in the synthetic FMs space or in real space. This can pave the way for numerous intriguing applications in integrated quantum computation and various information-processing tasks.

Finally, the exotic hybrid spectral features revealed herein, namely, *emerging diabolically degenerate exceptional points in the unfolded bosonic FMs space*, can motivate the construction of real-space Hamiltonians describing multimode systems with unique dynamical characteristics [55].

ACKNOWLEDGMENTS

A.M. is supported by the Polish National Science Centre (NCN) under the Maestro Grant No. DEC-2019/34/A/ST2/00081. S.K.O. acknowledges support from Air Force Office of Scientific Research (AFOSR) Multidisciplinary University Research Initiative (MURI) Award on Programmable systems with non-Hermitian quantum dynamics (Award No. FA9550-21-1-0202) and the AFOSR Award FA9550-18-1-0235. F.N. is supported in part by Nippon Telegraph and Telephone Corporation (NTT) Research, the Japan Science and Technology Agency (JST) [via the Quantum Leap Flagship Program (Q-LEAP), and the Moonshot R&D Grant No. JPMJMS2061], the Asian Office of Aerospace Research and Development (AOARD) (via Grant No. FA2386-20-1-4069), and the Foundational Questions Institute Fund (FQXi) via Grant No. FQXi-IAF19-06.

APPENDIX A: TENSOR PRODUCT STATES IN THE HIGHER-ORDER FIELD MOMENTS DYNAMICS OF QUADRATIC SYSTEMS: KRONECKER PRODUCTS AND SUMS

In this Appendix, we detail the construction of the evolution matrices for higher-order FMs based on the Kronecker sum operations and their eigendecomposition.

As we have already stressed, one of the remarkable features of quadratic systems is that one can obtain the analytical form of an evolution matrix ruling the dynamics of any higher-order FMs from the form of the evolution matrix M_1 for the

first-order FMs in Eq. (4). This can be done by exploiting some properties of matrices formed by Kronecker sums. First, we summarize the most important spectral features of Kronecker sum matrices in the following theorem.

Theorem. The eigenspectrum of a complex matrix $C \in \mathbb{C}^{(m+n) \times (m+n)}$, obtained as the Kronecker sum of two complex matrices $A \in \mathbb{C}^{m \times m}$ and $B \in \mathbb{C}^{n \times n}$, i.e., $C = A \oplus B = A \otimes I_B + I_A \otimes B$, has the form

$$\lambda(C) = \lambda(A) + \lambda(B), \quad \psi_C = \psi_A \otimes \psi_B, \quad (\text{A1})$$

where $\lambda(M)$ and ψ_M are the eigenvalues and eigenvectors of a matrix $M = A, B, C$, respectively.

Proof. The proof is straightforward. We start from the eigenvalue-eigenvector equation for the matrix C by feeding it into the equation for the right eigenvector, which is a tensor product of the two eigenvectors ψ_A and ψ_B , with eigenvalues $\lambda(A)$ and $\lambda(B)$, respectively. Namely,

$$\begin{aligned} C(\psi_A \otimes \psi_B) &= (A \oplus B)(\psi_A \otimes \psi_B) \\ &= (A \otimes I_B)(\psi_A \otimes \psi_B) + (I_A \otimes B)(\psi_A \otimes \psi_B) \\ &= (A\psi_A \otimes I_B\psi_B) + (I_A\psi_A \otimes B\psi_B) \\ &= (\lambda_A\psi_A \otimes \psi_B) + (\psi_A \otimes \lambda_B\psi_B) \\ &= (\lambda_A + \lambda_B)\psi_A \otimes \psi_B, \end{aligned} \quad (\text{A2})$$

where we used the tensor and dot product properties of matrices and vectors. In other words, the eigenvector of the matrix $C = A \oplus B$, corresponding to the eigenvalue $\lambda(C)$, is indeed just the tensor product of the two eigenvectors of the matrices A and B with eigenvalues $\lambda(A)$ and $\lambda(B)$.

According to Eq. (A2), the matrix, whose eigenvectors are formed by the tensor products of eigenvectors of two matrices, can be utilized in the construction of the evolution matrices of any higher order. To reveal how this works in practice, let us consider the second-order field moments. The various combinations of second-order field moments are obtained from the tensor product of the Nambu vector,

$$\hat{\Psi} = [\hat{a}_1, \hat{a}_2, \dots, \hat{a}_N, \hat{a}_1^\dagger, \hat{a}_2^\dagger, \dots, \hat{a}_N^\dagger]^T, \quad (\text{A3})$$

on itself, i.e., from the $4N^2$ -dimensional vector $\langle \hat{\Psi} \otimes \Psi \rangle$. According to Eq. (A2), the evolution matrix M_2 , governing the vector of the second-order FMs,

$$\frac{d}{dt} \langle \hat{\Psi} \otimes \Psi \rangle = M_2 \langle \hat{\Psi} \otimes \Psi \rangle, \quad (\text{A4})$$

attains the form

$$M_2 = M_1 \oplus M_1 = M_1 \otimes I_{2N} + I_{2N} \otimes M_1. \quad (\text{A5})$$

The form of the evolution matrix M_2 coincides, as it should, with that derived from the Lyapunov equation for the covariance matrix, when the latter is presented as a column vector [52]. This procedure can thus be iteratively continued to any m th-order field moment vectors $\langle \otimes_1^m \Psi \rangle$, thus obtaining Eq. (4).

The eigenvectors space for such evolution matrices M_m governing m th-order FMs can thus be represented as a tree structure, according to Eq. (6). For instance, for a dimer, this tree structure takes the form shown in Fig. 3.

APPENDIX B: DIMENSIONAL REDUCTION OF POLYTOPES TO SIMPLEXES IN THE FIELD-MOMENTS SPACE OF BOSONIC SYSTEMS

As we have already stressed, the highly degenerate eigenspace of a $(2N)^m \times (2N)^m$ matrix M_m can be effectively reduced to the nondegenerate space of a matrix M_m^{eff} of size $S_m(2N) \times S_m(2N)$. This space folding can be associated with the dimensional reduction of a polytope to a simplex. The reduction of the degenerate space can be performed in accordance with the following algorithm, which allows us to simultaneously retrieve both the reduced matrix M_m^{eff} and its eigenvectors.

(i) Define $(2N)^m \times (2N)^m$ matrices A and B , which consist of all the eigenvectors of M_m and basis vectors $v_k = [0, \dots, 1_k, \dots, 0]^T$, respectively: $A = [\psi_1, \dots, \psi_m]$ and $B = [v_1, \dots, v_m]$. The matrix B can thus be chosen as the identity matrix.

(ii) Eliminate all extra degenerate eigenvectors in A corresponding to a D_i -fold eigenvalue λ_i , such that among all the degenerate eigenmodes $\psi_{i_1, i_2, \dots, i_N}^{(N)}$ only one representative eigenvector

$$\psi^m(\lambda_i) = \frac{1}{D_i} \sum_{i_1, i_2, \dots, i_N} \psi_{i_1, i_2, \dots, i_N}^{(N)} \quad (\text{B1})$$

is left in the matrix. This transforms A to a matrix A' of the size $(2N)^m \times S_m$, which determines the nondegenerate eigenspace of M_m on which one wants to project.

(iii) Repeat the same procedure for the matrix $B \rightarrow B'$, collecting and eliminating the columns with the same indices as in the map $A \rightarrow A'$. Matrix B' defines the basis for the reduced matrix M_m^{eff} .

(iv) Project the $(2N)^m \times (2N)^m$ matrix M_m onto its nondegenerate $S_m(2N)$ -dimensional eigenspace spanned by the columns in A' , which results in the formation of a diagonal $S_m(2N) \times S_m(2N)$ matrix D . This can be done either by simply filling the diagonals of D with the corresponding eigenvalues λ of the column eigenvectors in A' , or more formally via the action $D = A''^\dagger M_m A'$, where A'' is dual to A' , with the property $A''^\dagger A' = I$, and which is comprised by the corresponding left eigenvectors of M_m .

(v) The matrix M_m^{eff} is then found as $M_m^{\text{eff}} = T D T^{-1}$, where the matrix $T = B'^T A'$, whose columns are comprised by the eigenvectors of M_m^{eff} .

Following these steps allows one to straightforwardly find the reduced effective matrix M_m^{eff} and its eigenvectors from the original high-dimensional matrix M_m .

APPENDIX C: EXAMPLE: QUANTUM PARAMETRIC SUBHARMONIC GENERATION PROCESSES

To explicitly illustrate the existence of IPCs with the tensor-product-states structure and diabatically degenerate exceptional points (DDEPs) in the FMs space of quadratic systems, we now consider the FM dynamics (up to third order) for parametric subharmonic generation processes. Previous works [65–67] have already revealed the existence of exceptional points (EPs) in such nondissipative quadratic Hamiltonians. Here, we show that such non-Hermitian

systems can possess additional nontrivial spectral features in the FMs space, i.e., DDEPs.

Let us first start from a quadratic Hermitian Hamiltonian \hat{H} describing a second subharmonic generation with a classical pump. Working in the reference frame rotating at the pump frequency ω_p ,

$$\hat{H} = \Delta \hat{a}^\dagger \hat{a} + (ig/2)(\hat{a}^2 - \hat{a}^{\dagger 2}), \quad (\text{C1})$$

where $\Delta = \omega_p - \omega$ is the resonance detuning, i.e., the difference between the frequencies of the pump (ω_p) and quantum field (ω), the parameter g is assumed to be a real-valued coupling constant, which involves the amplitude of the pump field [68].

1. First-order field-moments dynamics

The dynamics of the first-order moments of the Nambu operator vector $\hat{\Psi} = [\hat{a}, \hat{a}^\dagger]^T$ obey Eq. (4) with the evolution matrix

$$M_1 = \begin{pmatrix} -i\Delta & -g \\ -g & i\Delta \end{pmatrix}. \quad (\text{C2})$$

The matrix M_1 is \mathcal{PT} -symmetric [69,70], i.e., it is invariant under action $\mathcal{PT}M_1(\mathcal{PT})^{-1}$, of the parity \mathcal{P} and time-reversal (\mathcal{T}) operators, the action of which is defined as $\mathcal{PT} = \hat{\sigma}_x \mathcal{K}$, where the operator \mathcal{K} accounts for the complex conjugate operation. The symmetric matrix M_1 describes a complex 1-polytope, shown in Fig. 1(a), with two vertices having complex weights $\pm i\Delta$ and a single edge with weight $-g$. The eigenvalues of M_1 are $\lambda_{1,2} = \pm \Lambda$, where $\Lambda = \sqrt{g^2 - \Delta^2}$. The corresponding first-order moment eigenvectors become

$$\psi_{1,2} \equiv \begin{pmatrix} \mp \exp(\mp i\phi) \\ 1 \end{pmatrix}, \quad \phi = \arctan(\Delta/\Lambda), \quad (\text{C3})$$

which satisfy biorthogonality. Both the eigenvalues and eigenvectors coalesce at the second-order EP, defined by the condition $g_{\text{EP}} = \Delta$, with the phase $\phi_{\text{EP}} = \pi(2k+1)/2$, $k \in \mathbb{Z}$, in Eq. (C3).

2. Second-order field-moments dynamics

The evolution matrix M_2 , governing the second-order FM vector

$$\langle \hat{\Psi} \otimes \hat{\Psi} \rangle = [\langle \hat{a}^2 \rangle, \langle \hat{a} \hat{a}^\dagger \rangle, \langle \hat{a}^\dagger \hat{a} \rangle, \langle \hat{a}^{\dagger 2} \rangle]^T, \quad (\text{C4})$$

and describing a 2-polytope in the form of a square [see Fig. 1(a)], reads

$$M_2 = \begin{pmatrix} -2i\Delta & -g & -g & 0 \\ -g & 0 & 0 & -g \\ -g & 0 & 0 & -g \\ 0 & -g & -g & 2i\Delta \end{pmatrix}. \quad (\text{C5})$$

The eigenvalues of M_2 are $\lambda_{jk}^{(2)} = 2\Lambda \text{diag}[1, -1]$, where all four eigenvalues are listed in matrix form, with $j, k = 1, 2$.

The eigenvectors of M_2 are then obtained via all $2^2 = 4$ combinations of tensor products of the eigenvectors $\psi_{1,2}$ in Eq. (C3), according to Eq. (6):

$$\psi_{i_1, i_2}^{(2)} = \psi_{i_1} \otimes \psi_{i_2}, \tag{C6}$$

where each index $i_k = 1, 2$, for each $k = 1, 2$. Namely,

$$\psi^{(2)} = \begin{pmatrix} e^{-2i\phi} & -1 & -1 & e^{2i\phi} \\ -e^{-i\phi} & -e^{-i\phi} & e^{i\phi} & e^{i\phi} \\ -e^{-i\phi} & e^{i\phi} & -e^{-i\phi} & e^{i\phi} \\ 1 & 1 & 1 & 1 \end{pmatrix}. \tag{C7}$$

The matrix M_2 possesses only a single nondegenerate exceptional point (NDEP) of third order, i.e., there is no DDEP in the second-order FM space.

Below we comment on the reduction of the degenerate dimensions in the IPC to the ISC in the second-order FMs space of the system considered. The twofold-degenerate eigenvalue $\lambda_{12}^{(2)} = \lambda_{21}^{(2)} = 0$ arises because of the redundant moment elements $\langle \hat{a}\hat{a}^\dagger \rangle$ and $\langle \hat{a}^\dagger \hat{a} \rangle$ in the moments vector $\langle \hat{\Psi} \otimes \hat{\Psi} \rangle$. As such, the ($2^2 = 4$)-dimensional eigenspace of the second-order moments can be decreased to an [$S_2(2) = 3$]-dimensional one.

(i) The matrix A has the same form as in Eq. (C7). The matrix B is just an identity matrix, i.e., $B = I_4$.

(ii) Since only two eigenvectors [the second and third columns in Eq. (C7)]

$$\begin{aligned} \psi_2 &= [-1, -e^{-i\phi}, e^{i\phi}, 1]^T, \\ \psi_3 &= [-1, e^{i\phi}, -e^{-i\phi}, 1]^T \end{aligned} \tag{C8}$$

are degenerate, belonging to the zero-valued eigenvalue, we construct a new eigenvector $\psi = (\psi_2 + \psi_3)/2$. Thus, we obtain a new 4×3 matrix A' ,

$$A' = \begin{pmatrix} e^{-2i\phi} & -1 & e^{2i\phi} \\ -e^{-i\phi} & i \sin \phi & e^{i\phi} \\ -e^{-i\phi} & i \sin \phi & e^{i\phi} \\ 1 & 1 & 1 \end{pmatrix}. \tag{C9}$$

(iii) Similarly, one attains the matrix B' as follows:

$$B' = \begin{pmatrix} 1 & 0 & 0 \\ 0 & 1/2 & 0 \\ 0 & 1/2 & 0 \\ 0 & 0 & 1 \end{pmatrix}. \tag{C10}$$

(iv) The 3×3 diagonal matrix D then reads

$$D = \text{diag}[\Lambda, 0, -\Lambda]. \tag{C11}$$

(v) By constructing the matrix $T = B'^T A'$ in the form

$$T = \begin{pmatrix} e^{-2i\phi} & -1 & e^{2i\phi} \\ -e^{-i\phi} & i \sin(\phi) & e^{i\phi} \\ 1 & 1 & 1 \end{pmatrix}, \tag{C12}$$

one readily acquires the reduced effective matrix $M_2^{\text{eff}} = TDT^{-1}$, which reads

$$M_2^{\text{eff}} = \begin{pmatrix} -2i\Delta & -2g & 0 \\ -g & 0 & -g \\ 0 & -2g & 2i\Delta \end{pmatrix}. \tag{C13}$$

The eigenvectors of the matrix M_2^{eff} are, respectively, the columns of the matrix T .

3. Diablic degeneracy in the eigenspace of the third-order field moments: Diabolically degenerate exceptional points

Let us now elaborate in detail on the appearance of a DDEP in the third-order FMs space. The corresponding 8×8 evolution matrix M_3 , describing the dynamics of the vector of moments $\langle \bigotimes_1^3 \hat{\Psi} \rangle$ defined as

$$\begin{aligned} \left\langle \bigotimes_1^3 \hat{\Psi} \right\rangle &= [\langle \hat{a}^3 \rangle, \langle \hat{a}^2 \hat{a}^\dagger \rangle, \langle \hat{a} \hat{a}^\dagger \hat{a} \rangle, \langle \hat{a} \hat{a}^{\dagger 2} \rangle, \langle \hat{a}^\dagger \hat{a}^2 \rangle, \langle \hat{a}^\dagger \hat{a} \hat{a}^\dagger \rangle, \\ &\quad \langle \hat{a}^{\dagger 2} \hat{a} \rangle, \langle \hat{a}^{\dagger 3} \rangle]^T \end{aligned} \tag{C14}$$

according to Eq. (4), reads

$$M_3 = \begin{pmatrix} -3i\Delta & -g & -g & 0 & -g & 0 & 0 & 0 \\ -g & -i\Delta & 0 & -g & 0 & -g & 0 & 0 \\ -g & 0 & -i\Delta & -g & 0 & 0 & -g & 0 \\ 0 & -g & -g & i\Delta & 0 & 0 & 0 & -g \\ -g & 0 & 0 & 0 & -i\Delta & -g & -g & 0 \\ 0 & -g & 0 & 0 & -g & i\Delta & 0 & -g \\ 0 & 0 & -g & 0 & -g & 0 & i\Delta & -g \\ 0 & 0 & 0 & -g & 0 & -g & -g & 3i\Delta \end{pmatrix}. \tag{C15}$$

Its eigenvalues λ_{ijk} , according to Eq. (6) in the main text, can be listed as

$$\lambda^{(3)} = \begin{pmatrix} \lambda_{111} & \lambda_{112} & \lambda_{121} & \lambda_{122} & \lambda_{211} & \lambda_{212} & \lambda_{221} & \lambda_{222} \\ 3\Lambda & \Lambda & \Lambda & -\Lambda & \Lambda & -\Lambda & -\Lambda & -3\Lambda \end{pmatrix}, \tag{C16}$$

where as before $\Lambda = \sqrt{g^2 - \Delta^2}$. The corresponding eigenvectors are easily found, according to Eq. (6),

$$\psi^{(3)} = \begin{pmatrix} -e^{-3i\phi} & e^{-i\phi} & e^{-i\phi} & -e^{i\phi} & e^{-i\phi} & -e^{i\phi} & -e^{i\phi} & e^{3i\phi} \\ e^{-2i\phi} & e^{-2i\phi} & -1 & -1 & -1 & -1 & e^{2i\phi} & e^{2i\phi} \\ e^{-2i\phi} & -1 & e^{-2i\phi} & -1 & -1 & e^{2i\phi} & -1 & e^{2i\phi} \\ -e^{-i\phi} & -e^{-i\phi} & -e^{-i\phi} & -e^{-i\phi} & e^{i\phi} & e^{i\phi} & e^{i\phi} & e^{i\phi} \\ e^{-2i\phi} & -1 & -1 & e^{2i\phi} & e^{-2i\phi} & -1 & -1 & e^{2i\phi} \\ -e^{-i\phi} & -e^{-i\phi} & e^{i\phi} & e^{i\phi} & -e^{-i\phi} & -e^{-i\phi} & e^{i\phi} & e^{i\phi} \\ -e^{-i\phi} & e^{i\phi} & -e^{-i\phi} & e^{i\phi} & -e^{-i\phi} & e^{i\phi} & -e^{-i\phi} & e^{i\phi} \\ 1 & 1 & 1 & 1 & 1 & 1 & 1 & 1 \end{pmatrix}. \quad (\text{C17})$$

Note that the two eigenvalues $\pm\Lambda$ are triply degenerate. At the EP $g = \Delta$, the Jordan form of M_3 reads

$$M_3^{\text{EP}} = \begin{pmatrix} 0 & 1 & 0 & 0 & 0 & 0 & 0 & 0 \\ 0 & 0 & 1 & 0 & 0 & 0 & 0 & 0 \\ 0 & 0 & 0 & 1 & 0 & 0 & 0 & 0 \\ 0 & 0 & 0 & 0 & 0 & 0 & 0 & 0 \\ 0 & 0 & 0 & 0 & 0 & 1 & 0 & 0 \\ 0 & 0 & 0 & 0 & 0 & 0 & 0 & 0 \\ 0 & 0 & 0 & 0 & 0 & 0 & 0 & 1 \\ 0 & 0 & 0 & 0 & 0 & 0 & 0 & 0 \end{pmatrix}. \quad (\text{C18})$$

The effective dimension of M_3 is 4 [$S_3(2) = 4$], and, therefore, there is a single EP of fourth order. However, apart from this EP, also one DDEP of second order emerges, due to the triply degenerated pairs of eigenvalues.

To lift the degeneracy of the DDEP, one can induce a specific perturbation to the matrix M_3 , i.e., $M_3 \rightarrow M_3 + \epsilon P$, where ϵ denotes the perturbation strength. The matrix P can read

$$P = \text{diag}[1, 0, 0, 1, 0, 1, 0, 0]. \quad (\text{C19})$$

The result of such a perturbation on the eigenvalues of M_3 is shown in Fig. 4. Other choices of perturbation do not necessarily lead to the DDEP detection. Note that the perturbation is actually fictitious because of the symmetry protection of the evolution matrix M_3 in the FM space. Indeed, by unfolding the evolution matrices M_3 from the first-order moments 2×2 matrix M_1 , it is impossible to attain such a perturbed matrix M_3 . However, the formation of such a DDEP in the spectrum can be checked by mapping the evolution matrix M_3 to a certain real-space photonic-lattice Hamiltonian.

Importantly, the above-revealed hybrid spectral features of FMs polytopes can also be exploited in the construction of similar non-Hermitian Hamiltonians in real space. For instance, one of the nontrivial outcomes of the presence of a DDEP in the spectrum of real multimode non-Hermitian Hamiltonians can be the implementation of a programmable multimode switch by dynamically encircling the DDEP [55]. A direct detection of DDEPs in the FMs space of a bosonic system can be performed by measuring bosonic commutators [71] and/or anomalous FMs [72]. The tensor-product-states structure of a FM space can also be recovered from

Cahill-Glauber s -ordered FMs, which can be obtained from the measured normally ordered moments using standard photon-detection schemes [68,73,74]. Note that our conclusions remain valid also for the quadrature field moments, which could be easier to access experimentally, e.g., via standard balanced homodyne detection [65,75].

APPENDIX D: TRIANGULAR AND TETRAHEDRAL NON-HERMITIAN LATTICE MODELS IN THE FIELD-MOMENTS SPACE OF THREE- AND FOUR-MODE SYSTEMS, RESPECTIVELY

1. Triangular non-Hermitian lattice model with open boundaries

We have already mentioned the emergence of a triangular lattice in the FMs space of a three-mode system, as depicted in Fig. 3. Here we discuss in more detail the structure of such a lattice, its mapping to a non-Hermitian Hamiltonian, and we briefly mention the tetrahedral lattices appearing in the FMs space of four-mode systems.

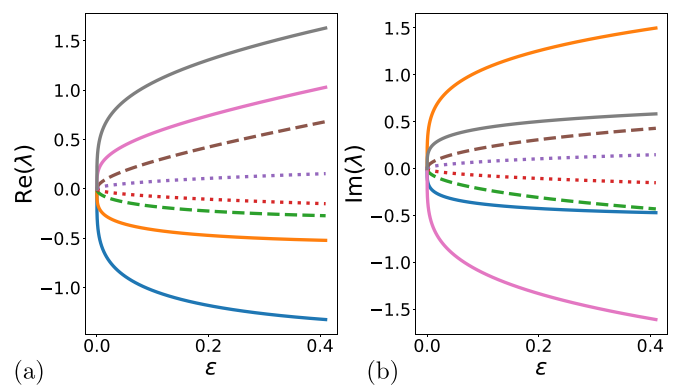


FIG. 4. Real (a) and imaginary (b) parts of the eigenvalues λ of the matrix M_3 , governing third-order FMs, at the EP $g = \Delta$, under the perturbation ϵ , which enables resolving a DDEP. The matrix M_3 has a single EP of fourth order (presented by the coalescence of four solid curves, characterized by the quartic-root dependence on perturbation, $\sqrt[4]{\epsilon}$). Apart from it, under the perturbation, the initial DDEP splits into two EPs of second order (presented by the merge of two eigenvalues, shown by the two dashed and two dotted curves, respectively, which are characterized by the square-root dependence of the perturbation, $\sqrt{\epsilon}$).

For the sake of clarity, we repeat some parts of the main text. First, let us consider the first-order FMs vector $\langle \hat{\Phi} \rangle$ of a three-mode system, where $\hat{\Phi} = [\hat{a}_1, \hat{a}_2, \hat{a}_3]^T$, which is governed by the following symmetric evolution matrix:

$$M_1 = \begin{pmatrix} \Delta_1 & \alpha & \gamma \\ \alpha & \Delta_2 & \beta \\ \gamma & \beta & \Delta_3 \end{pmatrix}. \quad (\text{D1})$$

Compared to Eq. (10), we also add the diagonal terms Δ_k , which can be associated with different resonant (complex) frequencies of the interacting modes. The degenerate evolution matrix M_N governing the dynamics of the N th-order FM $\langle \otimes_1^N \hat{\Phi} \rangle$ is obtained from M_1 according to Eq. (4). The matrix M_N then describes a highly degenerate $2N$ -polytope [the case for $N = 1, 2$ is shown in Fig. 1(b)]. This extra degeneracy can be eliminated by effectively reducing the $2N$ -polytope with 3^N vertices to a two-dimensional triangular ISC having $S_N(3)$ vertices instead (see also Fig. 3). This folding procedure is accompanied by the reduction of the symmetric evolution matrix M_N to the asymmetric effective matrix M_N^{eff} .

One then can relate the effective evolution matrix M_N^{eff} to a non-Hermitian Hamiltonian describing a triangle-shaped triangular lattice (shown in Fig. 3). One can see that the hopping amplitudes have the maximal values for the sites on the boundary, being proportional to the size of the corresponding external or internal triangle lattice edges. The tunneling amplitudes are steadily decreasing when approaching the opposite sides of the triangular lattice, revealing the characteristic asymmetry in the site interactions, i.e., their path dependence. The eigendecomposition of the non-Hermitian Hamiltonian \hat{H}^N , which is identical to the matrix M_N^{eff} , directly follows from the eigendecomposition of the matrix M_N , as was discussed in the previous section. Since the spectrum of M_N can be readily calculated, so can the eigenspectrum of the non-Hermitian Hamiltonian \hat{H}^N .

Namely, by inducing the map $M_N^{\text{eff}} \rightarrow \hat{H}^N$, one attains

$$\hat{H}^N = \hat{H}_0^N + \hat{H}_{\text{int}}^N, \quad (\text{D2})$$

where \hat{H}_0^N accounts for the noninteracting Hamiltonian part describing ‘‘site potentials’’ on the triangular lattice, which reads

$$\hat{H}_0^N = \sum_{\substack{j,k=1 \\ l=N-j-k}}^N (j\Delta_1 + k\Delta_2 + l\Delta_3) \hat{c}_{j,k,l}^\dagger \hat{c}_{j,k,l}, \quad (\text{D3})$$

and asymmetric ‘‘site interactions’’ are described by

$$\begin{aligned} \hat{H}_{\text{int}}^N = & \sum_{\substack{j,k=1 \\ l=N-j-k}}^N \hat{c}_{j,k,l} (f_j^\alpha \hat{c}_{j-1,k+1,l}^\dagger + f_j^\gamma \hat{c}_{j-1,k,l+1}^\dagger \\ & + f_k^\beta \hat{c}_{j,k-1,l+1}^\dagger + f_k^\alpha \hat{c}_{j+1,k-1,l}^\dagger \\ & + f_l^\gamma \hat{c}_{j+1,k,l-1}^\dagger + f_l^\beta \hat{c}_{j,k+1,l-1}^\dagger) \\ & + \hat{c}_{j,k,l}^\dagger (f_{k+1}^\alpha \hat{c}_{j-1,k+1,l} + f_{l+1}^\gamma \hat{c}_{j-1,k,l+1} \\ & + f_{l+1}^\beta \hat{c}_{j,k-1,l+1} + f_{j+1}^\alpha \hat{c}_{j+1,k-1,l} \\ & + f_{j+1}^\gamma \hat{c}_{j+1,k,l-1} + f_{k+1}^\beta \hat{c}_{j,k+1,l-1}), \end{aligned} \quad (\text{D4})$$

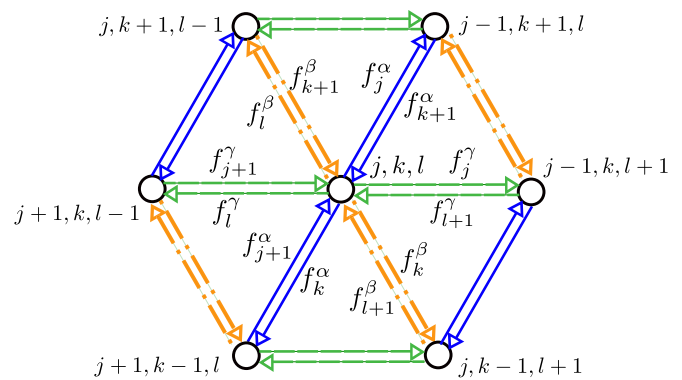


FIG. 5. An element of the triangular non-Hermitian lattice model in Fig. 3(c), described by the non-Hermitian Hamiltonian in Eq. (D2), illustrating the nearest-neighbor interactions for a site with indices (j, k, l) (shown in the center). The site potentials and couplings f_q^ξ are given in Eqs. (D3) and (D4), respectively.

where the hopping coefficients read $f_q^\xi = q\xi$. An element of such a lattice is also shown in Fig. 5.

2. Tetrahedral non-Hermitian lattice model with open boundaries

In a similar fashion, one can obtain a 3-simplex non-Hermitian lattice, namely a non-Hermitian tetrahedral-octahedral honeycomb model, emerging in the ISCc FMs space of a four-mode system, whose first-order FMs symmetric evolution matrix has the following generic form:

$$M_1 = \begin{pmatrix} \Delta_1 & \alpha & \gamma & \mu \\ \alpha & \Delta_2 & \beta & \xi \\ \gamma & \beta & \Delta_3 & \nu \\ \mu & \xi & \nu & \Delta_4 \end{pmatrix}. \quad (\text{D5})$$

The schematic representation of the 3-simplex described by the matrix M_1 is shown in Fig. 6(a). The second-order FMs evolution matrix M_2 is then an augmented tetrahedron from below [see Fig. 6(b)]. Similarly, one obtains an iterated 3-simplex chain comprised by tetrahedrons for arbitrarily high-order FMs.

APPENDIX E: SYMMETRIZATION OF NON-HERMITIAN n -SIMPLEX LATTICES

As was mentioned in Secs. II E and III of the main text, the asymmetric n -simplex lattices, emerging in the FMS of quadratic systems, can be transformed into symmetric ones by finding an appropriate similarity transformation, or, in other words, by choosing an appropriate basis when performing a projection of IPCs onto ISCs. This means that because of such lattice symmetrization, only eigenvectors are modified, whereas eigenvalues are left the same.

In point (iii) of Appendix B, we have pointed out that a general $(2N)^m \times S_m(2N)$ matrix B' , which defines the basis of the polytopes projection on their nondegenerate space, is composed of S_m column-vectors, where S_m is given in Eq. (8). Some of these column-vectors are formed as a symmetrical combination, i.e., an average, of column-vectors of the

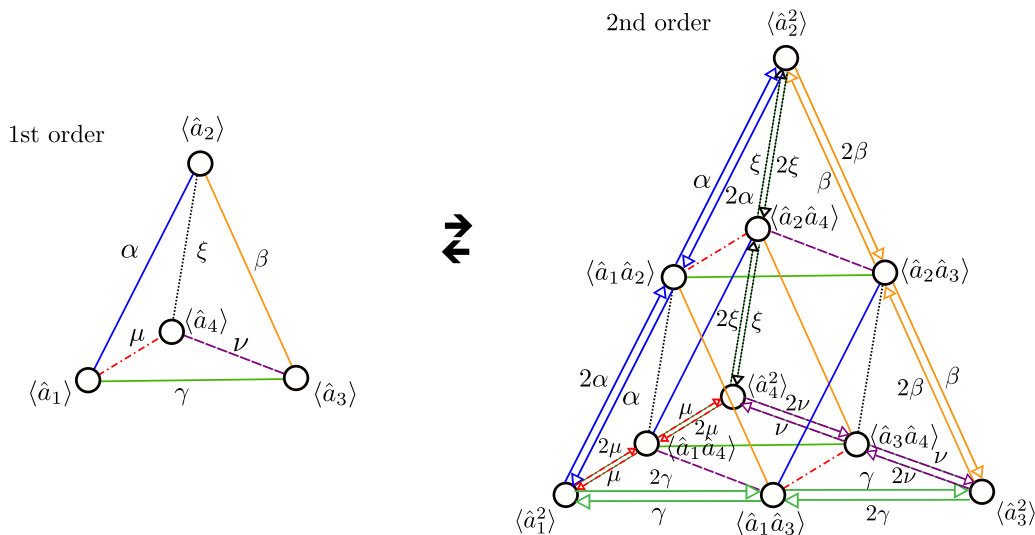


FIG. 6. Formation of iterated simplex chains by folding iterated polytope chains in the field-moments space of bosonic four-mode systems. (a) A 3-simplex, i.e., a tetrahedron, formed in the first-order FMs, which coincides with the P_{i_1} polytope. The links, denoted by Greek letters $\alpha, \beta, \gamma, \mu, \xi, \nu$, and highlighted by different colors, correspond to the coupling strengths between the three FMs. (b) An ISC in the second-order FMs space. By folding the corresponding symmetric 6-polytope, one obtains an asymmetric 3-simplex, namely a tetrahedral-octahedral honeycomb in the high-order FMs space of the four-mode bosonic system.

identity matrix $I_{(2N)^m}$. However, if instead of that “average” of D_i basis vectors, factored by $1/D_i$ [see Eq. (B1)], we take the same combination but factored by $1/\sqrt{D_i}$, i.e., a normalized sum, then the new resulting transformation matrix $T = B^T A'$ would produce a symmetric effective matrix M_m^{eff} , which describes the symmetrized n -simplex lattice.

Let us explain this in more detail by considering a simple example, similar to that in Appendix C2. That is, we would like to symmetrize the matrix M_2^{eff} in Eq. (C13). For that, instead of the matrix B' , in Eq. (C10), we take a new matrix

B'' , now formed by *normalized* column-vectors, i.e.,

$$B' \rightarrow B'' = \begin{pmatrix} 1 & 0 & 0 \\ 0 & \frac{1}{\sqrt{2}} & 0 \\ 0 & \frac{1}{\sqrt{2}} & 0 \\ 0 & 0 & 1 \end{pmatrix}. \tag{E1}$$

By constructing a modified transformation matrix $T' = B''^T A'$, where A' is the same as in Eq. (C9), one obtains the

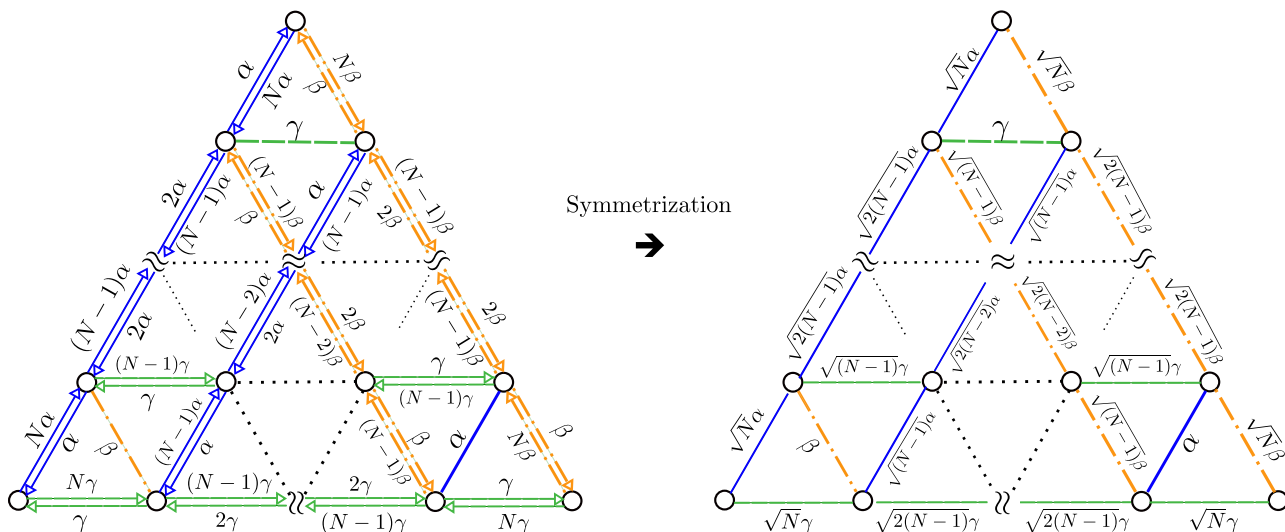


FIG. 7. Symmetrization of the asymmetric 2-simplex lattice (left panel), also shown in Fig. 3(c), to the symmetric 2-simplex lattice (right panel). In other words, the asymmetric intersite couplings (depicted as double arrows on the left panel) become symmetric (shown by single arrows on the right panel). This mapping can be realized via an appropriate similarity transformation, or, alternatively, by choosing an appropriate basis when projecting polytopes onto simplexes, formed in the field-moments space of quadratic systems. The edges of the symmetric 2-simplex lattice can describe a quantum angular momentum operator with different quantum numbers. See more details in Appendix E.

symmetrical matrix $M_{2,\text{sym}}^{\text{eff}}$ in the form

$$M_{2,\text{sym}}^{\text{eff}} = T'DT'^{-1} = \begin{pmatrix} -2i\Delta & -\sqrt{2}g & 0 \\ -\sqrt{2}g & 0 & -\sqrt{2}g \\ 0 & -\sqrt{2}g & 2i\Delta \end{pmatrix}, \quad (\text{E2})$$

where diagonal matrix D is given in Eq. (C11). For a two-mode system, one can then show that an arbitrary M_m^{eff} matrix is similar to the symmetric matrix $M_{m,\text{sym}}^{\text{eff}}$ via the transformation in Eq. (13).

One can straightforwardly verify that this symmetrization procedure is extended to any effective matrix M_m^{eff} describing an n -simplex lattice. For instance, for a 2-simplex lattice, with asymmetrical bidirectional links as shown in Fig. 3(c), the described symmetrization procedure allows us to transform that lattice into a symmetrical one, where the intersite couplings become symmetric (see Fig. 7).

Remarkably, due to this symmetrization of M_m^{eff} , the resulting symmetric n -simplex lattices have 1D edges which can be mapped to the angular-momentum operator \hat{J}_z in the Fock space representation (up to a certain scaling factor, proportional to a bosonic mode coupling), provided that the diagonal elements of M_m^{eff} are zero. Indeed, according to Fig. 7, all (anti-)diagonal and horizontal edges of the symmetric 2-simplex lattice can represent the angular momentum operator with a certain azimuthal quantum number j , which is determined by the number of vertices belonging to the corresponding edge.

For instance, the submatrices of M_m^{eff} describing three outer edges in Fig. 7, which contain $(N + 1)$ vertices, correspond to the angular momentum operator with the quantum number $j = N/2$ (see also Sec. III), with additional scaling factors α , β , and γ (see Fig. 7). In general, an edge having K vertices is related to the angular-momentum quantum number $j = (K - 1)/2$ (see Fig. 7).

-
- [1] M. Aizenman and E. Lieb, The third law of thermodynamics and the degeneracy of the ground state for lattice systems, *J. Stat. Phys.* **24**, 279 (1981).
- [2] X. Wu, N. Izmailian, and W. Guo, Shape-dependent finite-size effect of the critical two-dimensional Ising model on a triangular lattice, *Phys. Rev. E* **87**, 022124 (2013).
- [3] R. J. Baxter, The bulk, surface and corner free energies of the anisotropic triangular Ising model, *Proc. R. Soc. A* **476**, 20190713 (2020).
- [4] N. Hatano and D. R. Nelson, Localization transitions in non-hermitian quantum mechanics, *Phys. Rev. Lett.* **77**, 570 (1996).
- [5] Y. Ashida, Z. Gong, and M. Ueda, Non-Hermitian physics, *Adv. Phys.* **69**, 249 (2020).
- [6] E. J. Bergholtz, J. C. Budich, and F. K. Kunst, Exceptional topology of non-Hermitian systems, *Rev. Mod. Phys.* **93**, 015005 (2021).
- [7] K. Ding, C. Fang, and G. Ma, Non-Hermitian topology and exceptional-point geometries, *Nat. Rev. Phys.* **4**, 745 (2022).
- [8] H. Scheffé, Experiments with mixtures, *J. R. Stat. Soc. B* **20**, 344 (1958).
- [9] P. K. Luther and J. M. Squire, Three-dimensional structure of the vertebrate muscle A-band: II. The myosin filament superlattice, *J. Mol. Biol.* **141**, 409 (1980).
- [10] B. Grünbaum, *Convex Polytopes*, 2nd ed. (Springer, New York, 2003).
- [11] D. R. Nelson and M. Widom, Symmetry, Landau theory and polytope models of glass, *Nucl. Phys. B* **240**, 113 (1984).
- [12] R. J. Baxter, Exactly solved models in statistical mechanics, in *Integrable Systems in Statistical Mechanics* (World Scientific, 1985), pp. 5–63.
- [13] *Classical and Quantum Nonlinear Integrable Systems: Theory and Application*, edited by A. Kundu (CRC, Boca Raton, FL, 2003).
- [14] A. Kitaev, Anyons in an exactly solved model and beyond, *Ann. Phys.* **321**, 2 (2006).
- [15] H. Yao and S. A. Kivelson, Exact chiral spin liquid with non-abelian anyons, *Phys. Rev. Lett.* **99**, 247203 (2007).
- [16] Z. Nussinov and G. Ortiz, Bond algebras and exact solvability of Hamiltonians: Spin $s = \frac{1}{2}$ multilayer systems, *Phys. Rev. B* **79**, 214440 (2009).
- [17] N. Leumer, M. Marganska, B. Muralidharan, and M. Grifoni, Exact eigenvectors and eigenvalues of the finite Kitaev chain and its topological properties, *J. Phys.: Condens. Matter* **32**, 445502 (2020).
- [18] R. Orús, Tensor networks for complex quantum systems, *Nat. Rev. Phys.* **1**, 538 (2019).
- [19] G. Carleo *et al.*, Machine learning and the physical sciences, *Rev. Mod. Phys.* **91**, 045002 (2019).
- [20] P. A. Kalugin, A. Y. Kitaev, and L. S. Levitov, $\text{Al}_{0.86}\text{Mn}_{0.14}$: A six-dimensional crystal, *Pis'ma Zh. Eksp. Teor. Phys.* **41**, 119 (1985) [*JETP Lett.* **41**, 145 (1985)].
- [21] V. Elser, Indexing problems in quasicrystal diffraction, *Phys. Rev. B* **32**, 4892 (1985).
- [22] A. Katz and M. Duneau, Quasiperiodic patterns and icosahedral symmetry, *J. Phys. France* **47**, 181 (1986).
- [23] F. Nori, M. Ronchetti, and V. Elser, Strain accumulation in quasicrystalline solids, *Phys. Rev. Lett.* **61**, 2774 (1988).
- [24] M. Baake, D. Joseph, and P. Kramer, The Schur rotation as a simple approach to the transition between quasiperiodic and periodic phases, *J. Phys. A* **24**, L961 (1991).
- [25] L. M. Narducci and M. Orszag, Eigenvalues and eigenvectors of angular momentum operator J_x without the theory of rotations, *Am. J. Phys.* **40**, 1811 (1972).
- [26] Z. Hu, Eigenvalues and eigenvectors of a class of irreducible tridiagonal matrices, *Lin. Alg. Appl.* **619**, 328 (2021).
- [27] Y. N. Joglekar and A. Saxena, Robust \mathcal{PT} -symmetric chain and properties of its Hermitian counterpart, *Phys. Rev. A* **83**, 050101(R) (2011).
- [28] I. I. Arkhipov and F. Minganti, Emergent non-Hermitian localization phenomena in the synthetic space of zero-dimensional bosonic systems, *Phys. Rev. A* **107**, 012202 (2023).
- [29] A. J. Daley, I. Bloch, C. Kokail *et al.*, Practical quantum advantage in quantum simulation, *Nature (London)* **607**, 667 (2022).

- [30] F. Nori and Y.-L. Lin, Analytical solution for the Fermi-sea energy of two-dimensional electrons in a magnetic field: Lattice path-integral approach and quantum interference, *Phys. Rev. B* **49**, 4131 (1994).
- [31] Y.-L. Lin and F. Nori, Quantum interference from sums over closed paths for electrons on a three-dimensional lattice in a magnetic field: Total energy, magnetic moment, and orbital susceptibility, *Phys. Rev. B* **53**, 13374 (1996).
- [32] Y.-L. Lin and F. Nori, Strongly localized electrons in a magnetic field: exact results on quantum interference and magnetoconductance, *Phys. Rev. Lett.* **76**, 4580 (1996).
- [33] Y.-L. Lin and F. Nori, Analytical results on quantum interference and magnetoconductance for strongly localized electrons in a magnetic field: Exact summation of forward-scattering paths, *Phys. Rev. B* **53**, 15543 (1996).
- [34] Y.-L. Lin and F. Nori, Quantum interference in superconducting wire networks and Josephson junction arrays: An analytical approach based on multiple-loop Aharonov-Bohm Feynman path integrals, *Phys. Rev. B* **65**, 214504 (2002).
- [35] A. Regensburger, C. Bersch, M.-A. Miri, G. Onishchukov, D. N. Christodoulides, and U. Peschel, Parity-time synthetic photonic lattices, *Nature (London)* **488**, 167 (2012).
- [36] L. Yuan, Q. Lin, M. Xiao, and S. Fan, Synthetic dimension in photonics, *Optica* **5**, 1396 (2018).
- [37] T. Ozawa and H. M. Price, Topological quantum matter in synthetic dimensions, *Nat. Rev. Phys.* **1**, 349 (2019).
- [38] E. Lustig, S. Weimann, Y. Plotnik, Y. Lumer, M. A. Bandres, A. Szameit, and M. Segev, Photonic topological insulator in synthetic dimensions, *Nature (London)* **567**, 356 (2019).
- [39] A. Fabre, J.-B. Bouhiron, T. Satoor, R. Lopes, and S. Nascimbene, Simulating two-dimensional dynamics within a large-size atomic spin, *Phys. Rev. A* **105**, 013301 (2022).
- [40] S. Weimann, M. Kremer, Y. Plotnik, Y. Lumer, S. Nolte, K. Makris, M. Segev, M. Rechtsman, and A. Szameit, Topologically protected bound states in photonic parity-time-symmetric crystals, *Nat. Mater.* **16**, 433 (2017).
- [41] A. Roy, M. Parto, R. Nehra, C. Leefmans, and A. Marandi, Topological optical parametric oscillation, *Nanophotonics* **11**, 1611 (2022).
- [42] S. Weidemann, M. Kremer, T. Helbig, T. Hofmann, A. Stegmaier, M. Greiter, R. Thomale, and A. Szameit, Topological funneling of light, *Science* **368**, 311 (2020).
- [43] M. H. Teimourpour, R. El-Ganainy, A. Eisfeld, A. Szameit, and D. N. Christodoulides, Light transport in \mathcal{PT} -invariant photonic structures with hidden symmetries, *Phys. Rev. A* **90**, 053817 (2014).
- [44] M. A. Quiroz-Juárez, A. Perez-Leija, K. Tschernig, B. M. Rodríguez-Lara, O. S. Magaña-Loaiza, K. Busch, Y. N. Joglekar, and R. J. León-Montiel, Exceptional points of any order in a single, lossy waveguide beam splitter by photon-number-resolved detection, *Photon. Res.* **7**, 862 (2019).
- [45] K. Tschernig, R. J. León-Montiel, A. Pérez-Leija, and K. Busch, Multiphoton synthetic lattices in multiport waveguide arrays: synthetic atoms and Fock graphs, *Photon. Res.* **8**, 1161 (2020).
- [46] P. Kok, W. J. Munro, K. Nemoto, T. C. Ralph, J. P. Dowling, and G. J. Milburn, Linear optical quantum computing with photonic qubits, *Rev. Mod. Phys.* **79**, 135 (2007).
- [47] I. I. Arkhipov, F. Minganti, A. Miranowicz, and F. Nori, Generating high-order quantum exceptional points in synthetic dimensions, *Phys. Rev. A* **104**, 012205 (2021).
- [48] C. Candan, M. Kutay, and H. Ozaktas, The discrete fractional Fourier transform, *IEEE Trans. Sign. Proc.* **48**, 1329 (2000).
- [49] S. Weimann, A. Perez-Leija, M. Lebugle *et al.*, Implementation of quantum and classical discrete fractional Fourier transforms, *Nat. Commun.* **7**, 11027 (2016).
- [50] Y. Zhou, M. Mirhosseini, D. Fu, J. Zhao, S. M. Hashemi Rafsanjani, A. E. Willner, and R. W. Boyd, Sorting photons by radial quantum number, *Phys. Rev. Lett.* **119**, 263602 (2017).
- [51] B. Niewelt, M. Jastrzębski, S. Kurzyrna, J. Nowosielski, W. Wasilewski, M. Mazelanik, and M. Parniak, Experimental implementation of the optical fractional fourier transform in the time-frequency domain, *Phys. Rev. Lett.* **130**, 240801 (2023).
- [52] S. Lototsky, Simple spectral bounds for sums of certain Kronecker products, *Lin. Alg. Appl.* **469**, 114 (2015).
- [53] J. Perina Jr., A. Miranowicz, G. Chimczak, and A. Kowalewska-Kudlaszyk, Quantum Liouvillian exceptional and diabolical points for bosonic fields with quadratic Hamiltonians: The Heisenberg-Langevin equation approach, *Quantum* **6**, 883 (2022).
- [54] Ş. K. Özdemir, S. Rotter, F. Nori, and L. Yang, Parity-time symmetry and exceptional points in photonics, *Nat. Mater.* **18**, 783 (2019).
- [55] I. I. Arkhipov, A. Miranowicz, F. Minganti, Ş. K. Özdemir, and F. Nori, Dynamically crossing diabolic points while encircling exceptional curves: A programmable symmetric-asymmetric multimode switch, *Nat. Commun.* **14**, 2076 (2023).
- [56] T. Kato, *Perturbation Theory for Linear Operators*, Classics in Mathematics (Springer, Berlin, 1995).
- [57] P. Doria, T. Calarco, and S. Montangero, Optimal control technique for many-body quantum dynamics, *Phys. Rev. Lett.* **106**, 190501 (2011).
- [58] N. Khaneja, T. Reiss, C. Kehlet, T. Schulte-Herbrüggen, and S. J. Glaser, Optimal control of coupled spin dynamics: design of NMR pulse sequences by gradient ascent algorithms, *J. Magn. Reson.* **172**, 296 (2005).
- [59] J. J. Sakurai and J. Napolitano, *Modern Quantum Mechanics* (Cambridge University Press, Cambridge, 2020).
- [60] M. Asano, R. Ohta, T. Aihara, T. Tsuchizawa, H. Okamoto, and H. Yamguchi, Optically probing Schwinger angular momenta in a micromechanical resonator, *Phys. Rev. A* **100**, 053801 (2019).
- [61] W. D. Heiss and A. L. Sannino, Transitional regions of finite Fermi systems and quantum chaos, *Phys. Rev. A* **43**, 4159 (1991).
- [62] G. C. Wick, The evaluation of the collision matrix, *Phys. Rev.* **80**, 268 (1950).
- [63] A. Jagannathan, The Fibonacci quasicrystal: Case study of hidden dimensions and multifractality, *Rev. Mod. Phys.* **93**, 045001 (2021).
- [64] K. Falconer, *Fractal Geometry: Mathematical Foundations and Applications* (Wiley, UK, 2014).
- [65] Y.-X. Wang and A. A. Clerk, Non-Hermitian dynamics without dissipation in quantum systems, *Phys. Rev. A* **99**, 063834 (2019).
- [66] A. Roy, S. Jahani, Q. Guo, A. Dutt, S. Fan, M.-A. Miri, and A. Marandi, Nondissipative non-Hermitian dynamics and

- exceptional points in coupled optical parametric oscillators, *Optica* **8**, 415 (2021).
- [67] V. P. Flynn, E. Cobanera, and L. Viola, Deconstructing effective non-Hermitian dynamics in quadratic bosonic Hamiltonians, *New J. Phys.* **22**, 083004 (2020).
- [68] J. Peřina, *Quantum Statistics of Linear and Nonlinear Optical Phenomena* (Kluwer, Dordrecht, 1991).
- [69] *Parity-time Symmetry and Its Applications*, edited by D. Christodoulides and J. Yang (Springer, Singapore, 2018).
- [70] R. El-Ganainy, K. G. Makris, M. Khajavikhan, Z. H. Musslimani, S. Rotter, and D. N. Christodoulides, Non-Hermitian physics and \mathcal{PT} symmetry, *Nat. Phys.* **14**, 11 (2018).
- [71] A. Zavatta, V. Parigi, M. S. Kim, H. Jeong, and M. Bellini, Experimental demonstration of the bosonic commutation relation via superpositions of quantum operations on thermal light fields, *Phys. Rev. Lett.* **103**, 140406 (2009).
- [72] B. Kühn, W. Vogel, M. Mraz, S. Köhnke, and B. Hage, Anomalous quantum correlations of squeezed light, *Phys. Rev. Lett.* **118**, 153601 (2017).
- [73] J. Peřina, I. I. Arkhipov, V. Michálek, and O. Haderka, Non-classicality and entanglement criteria for bipartite optical fields characterized by quadratic detectors, *Phys. Rev. A* **96**, 043845 (2017).
- [74] E. V. Shchukin and W. Vogel, Nonclassical moments and their measurement, *Phys. Rev. A* **72**, 043808 (2005).
- [75] F. Roccati, S. Lorenzo, G. M. Palma, G. T. Landi, M. Brunelli, and F. Ciccarello, Quantum correlations in \mathcal{PT} -symmetric systems, *Quantum Sci. Technol.* **6**, 025005 (2021).